Substitution effect of Me = Al, Bi, Cr and Mn to the microwave properties of polyaniline/BaMeFe 11 O 19 for absorbing electromagnetic waves

Tayssir Ben Ghzaiel, Wadia Dhaoui, Frédéric Schoenstein, Philippe Talbot, Frédéric Mazaleyrat

Substitution effect of *Me* = Al, Bi, Cr and Mn to the microwave properties of polyaniline/Ba*Me*$Fe_{11}O_{19}$ for absorbing electromagnetic waves

Tayssir BEN GHZAIEL[a,b], Wadia DHAOUI[a,*], Frédéric SCHOENSTEIN[c], Philippe TALBOT[d], Frédéric MAZALEYRAT[b]

[a] Université de Tunis El Manar Faculté des Sciences de Tunis, UR11ES18 Unité de Recherche de Chimie Minérale Appliquée, 2092, Tunis, Tunisie

[b] SATIE, ENS Cachan, CNRS, Université Paris-Saclay, 61 av du Président Wilson, F-94230 Cachan, France

[c] Université Paris XIII, Sorbonne Paris Cité, Laboratoire des Sciences des Procèdes et des Matériaux, LSPM, CNRS-UPR 3407, 99 Avenue J.B. Clement, 93430

[d] Lab-STICC UMR CNRS 6285, Université de Bretagne Occidentale, CS 93837, 6 avenue Le Gorgeu, 29238 Brest Cedex 3, France

*Corresponding author. Tel. +216 53 35 55 74

E-mail address: wadia.ammar@planet.tn

GRAPHICAL ABSTRACT

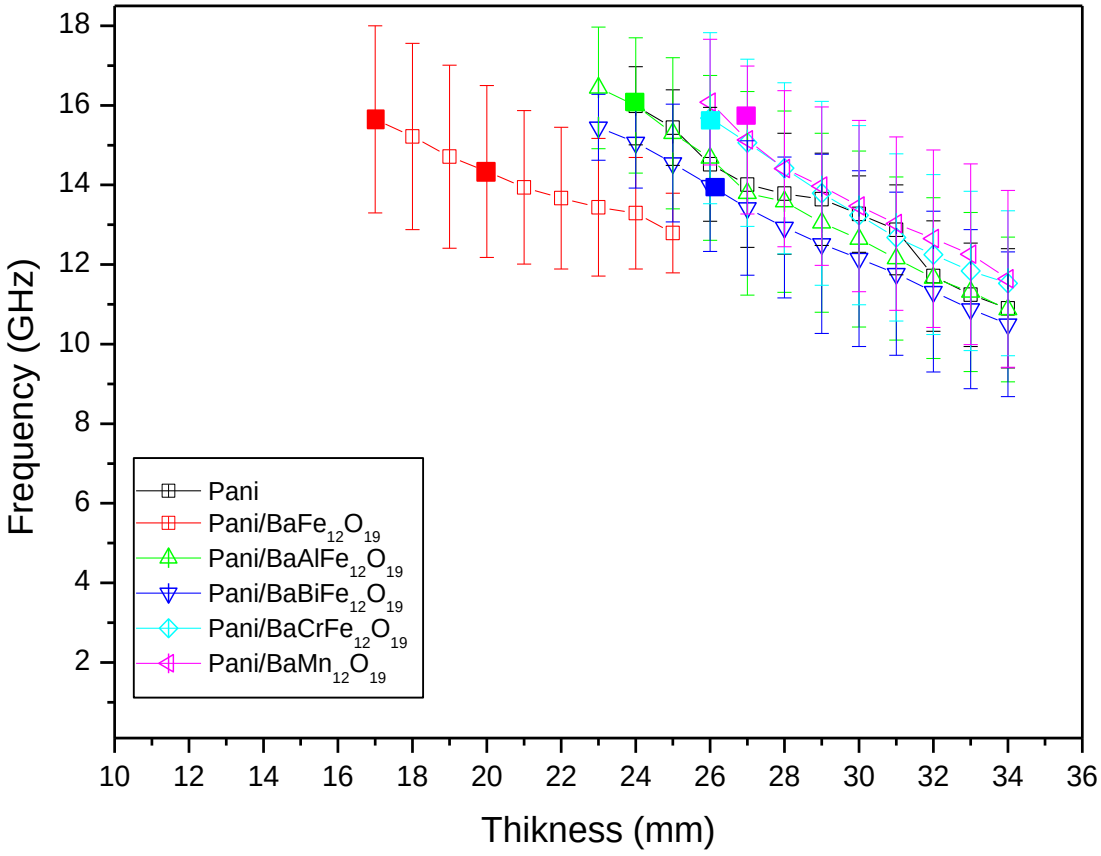

Abstract

Polyaniline/substituted barium hexaferrites (abbreviated Pani/Ba*Me*$Fe_{11}O_{19}$, where *Me*=Al, Bi, Cr and Mn) composites are investigated to be potential electromagnetic wave absorber from 1 to 18 GHz frequency range. Solid-Based Polymerization method is used to prepare the samples with 10 % volume fraction of hexaferrite. The effects of iron substitution in hexaferrite composites by trivalent ions Al^{3+}, Bi^{3+}, Cr^{3+} and Mn^{3+} on permittivity, permeability and microwave absorption properties are studied. Structural and morphological investigations confirm the presence of Polyaniline and barium hexaferrite phases, which are in interaction in the composites regardless the substitution. Thermogravimetric analysis exhibits an improved thermostability when small ions (Al^{3+} and Cr^{3+}) are used to substitute Fe^{3+} in hexaferrite compared to the large cations substitution (Bi^{3+} and Mn^{3+}), since these latter interfere between the ferrite and intermolecular interaction between Pani macromolecules. Magnetic studies show a ferromagnetic behaviour for all the composites. Saturation magnetization is mainly related to the substituting cations nature in hexaferrite which is determined using measured magnetic data. Coercivity values increase slightly due to the Pani matrix that precludes the movement of the domain wall. The EM parameters ε′, ε″, μ′and μ″ are measured using a Vector Network Analyzer. It is found that the dielectric constant increases with the addition of hexaferrite. The maximum of the magnetic losses diminishes and shifts to higher frequencies with Fe^{3+} doping. These measured EM parameters are used to determine the reflexion loss for different composites. Pani/$BaFe_{12}O_{19}$ composite shows two minimum reflection losses (RL) in Ku-band. The properties of these ferrites arise from exchange interactions between the oxygen and metallic ions occupying particular positions in its crystalline structure. For the

substituted ferrite composites, the minimum RL shifts from in Ku-band to X-band when substituting Fe^{3+} in hexaferrites by means of the variation of ferromagnetic resonance frequency which influences the microwave absorption properties.

Keywords: Polyaniline; A Composite Materials; B Solid State Reactions; C Magnetisation; D Thermal Analysis

1. Introduction

The increasing demand for high performance electromagnetic (EM) wave absorbing materials with high absorbing efficiency, wide absorption frequency range and light weight has aroused great interest in the development of the applications of electromagnetic wave at the high gigahertz (GHz) ranges including wireless telecommunication systems, radar, local area network, medical equipment,…[1-3]. Based on the magnetic loss or dielectric loss, a variety of absorbing materials have been designed such as conducting polymers, carbon nanotubes, ferrites,…[4-8]. Since single material can hardly satisfy these requirements, organic-inorganic conductive-magnetic composites are explored in order to develop new functional material joining the characteristics of the individual constituent which may enhance the absorption efficiency.

One of the most prevalent types of these composites is composed of Polyaniline (Pani) as conducting polymer and barium hexaferrite ($BaFe_{12}O_{19}$) as magnetic material [9, 10]. Due to the unique electrical conductivity, low density, easy preparation and good environmental stability, Polyaniline is considered as a promising candidate for electromagnetic wave absorbers [11, 12]. Nevertheless, pure Polyaniline presents a high complex permittivity and low complex permeability, resulting in a poor absorbance.

Therefore hexaferrites are often introduced in Pani to fabricate enhanced electromagnetic wave absorbers. Among ferrites, $BaFe_{12}O_{19}$ is a hard ferrimagnetic material which has interesting properties such as resonance absorption of moving magnetic domains, spin relaxation in the high-frequency alternating electromagnetic fields and thermal stability [13].

Intensive efforts have been devoted to develop techniques for the synthesis of nanocomposites; some of them, in situ polymerization [14], ultrasonic synthesis [15], emulsion polymerization [16] etc. However, only limited approaches have been used to develop simple, mild and efficient route to tune the properties of ferrite/Pani nanocomposites. Recently Solid-Based polymerization has emerged as a useful strategy for the fabrication of polymer-inorganic nanocomposites [17]. The solventless technique allows control of both structure and magnetic properties.

Barium hexaferrite-polymer composites, if formed by Solid-Based Polymerization route, have better compositional homogeneity and narrow particle size distribution compared to the composites obtained by standard Aqueous-Based Polymerization method as shown in our previous work [18].

From electromagnetic application point of view, the substituted barium ferrites are promising materials when they are used in polymer composites [19, 20]. Ion substitution in barium hexaferrite is interesting because of excellent magnetization, anisotropy, Curie temperature and the thermal stability. However, it is found that no much work has been reported on the dielectric and magnetic properties of trivalent iron substitution in barium ferrite-polymer composites in the high frequency region [21, 22].

The present work reports the synthesis of Polyaniline composites using Solid-Based Polymerization by incorporation of substituted barium ferrite particles $BaMeFe_{11}O_{19}$ (*Me* is an element in a trivalent state; Me^{3+} = Al^{3+}, Bi^{3+}, Cr^{3+} and Mn^{3+}) in Pani matrix. Substituting iron by Al, Bi, Cr and Mn is an effective way to vary the properties of barium ferrite. The reason for choosing those substituting ions is their different magnetic properties of their ferrites, according to our recently published study [23]. Complex permittivity, permeability and microwave absorption performance of the composites are studied in 1 - 18 GHz frequency range. The effects of iron substitution on ferrite and exchange coupling effect with Pani in the composites on the dielectric and magnetic losses are investigated by different measurement techniques to ensure the fabrication of the proper material for electromagnetic applications.

2. Experimental

2.1. Materials

$BaMeFe_{11}O_{19}$ hexaferrites (*Me*= Al, Bi, Cr and Mn) powders are prepared according to the previously reported method [18]. Aniline chloride (AnCl), ammonium peroxydisulfate ($(NH_4)_2S_2O_8$, APS) and hydrochloric acid (HCl) are all of analytical purity purchased from commercial sources, and used directly without further purification.

2.2. Preparation of Pani/Ba*Me*$Fe_{11}O_{19}$

Pani/Ba*Me*$Fe_{11}O_{19}$ composites are synthesized by Solid-Based Polymerization (solventless medium) according to the experimental procedure described elsewhere [18]. Initially, An-Cl and ferrite particles are ground in an agate mortar for 10 min. Subsequently, APS is added to the mixture and ground for 20 min until the colour

turned dark green. The molar ratio of aniline to APS is maintained at 1.25. The polymerization lasted for 24 h to complete the polymerization reaction at room temperature. The dark green product is washed by HCl (0.2 M) several times, filtered and then dried in a vacuum at 60 °C for 24 h. Since the effect of volume fraction has already been studied previously [18], we have fixed the volume fraction of ferrite at 10 %. Here, we are more interested to investigate the effect of the substitution iron on the properties of the composite. Pure Polyaniline is also synthesized under similar conditions as above.

2.3. Characterization

X-ray powder diffraction patterns are recorded using PANalytical X'Pert Pro diffractometer with Cobalt K_α radiation (λ = 1.79026 Å) at diffraction angle 2θ from 10 to 80° with 0.02° increment. The refining of X-Ray patterns was performed by Rietveld analysis [24] using MAUD software [25]. The morphology of the particles is observed by a Hitachi S-3400N Scanning Electron Microscopy (SEM). Fourier Transform Infrared spectra are collected on a Thermo Electron Corporation Nicolet Nexus 670 FT-IR Spectrometer over the range of 4000 - 400 cm^{-1} using KBr pellets. Thermal behaviour of the samples is examined by thermogravimetric analysis (TGA) using Perkin Elmer Pyris 6 TGA analyser at a heating rate of 10 °C. min^{-1} in nitrogen atmosphere. Magnetic properties of the composites are measured on vibrating sample magnetometer (VSM) Lake Shore 7400 model at room temperature. A vector network analyzer (Agilent network analyzer N6230A) is employed to determinate the values of the complex permittivity and permeability of the composites in a frequency range of 1 - 18 GHz by using coaxial reflexion/ transmission technique [26]. All the samples are compressed in the form of 7 mm outer diameter and 3 mm inner diameter rings.

3. Results and discussion

3.1. X-ray diffraction analysis

Fig. 1 (a - f) shows XRD patterns of pristine Pani and Pani/Ba*Me*$Fe_{11}O_{19}$ composites. Polyaniline (Fig. 1 a) reveals two broad diffraction peaks at 2 θ = 23.7° and 29.4° which are ascribed to the parallel and perpendicular periodicity of the polymer chains, respectively [27, 28]. The diffraction patterns for Pani composites, in Fig. 1 (b - f), present the characteristic peaks of Pani as well as those associated to barium hexaferrite. Independently of the nature of substituting ion, X-Ray diffraction analysis of all samples confirmed the presence of hexagonal M-type phase within space group $P6_{3/mmc}$ according to our previous work [18]. Furthermore, the major peaks values of this phase are indexed using JCPDS cards 74-1121 which proves that the substitution ions have occupied the crystal sites in the hexaferrite. The crystal phase of magnetic particles seems to be well maintained after the synthetic process of composites, based on the fact that there is no change in peak position between $BaFe_{12}O_{19}$ and the composites. It should be noted that the intensity of characteristic diffraction peaks of the polymer in the composites is weaker compared to the pristine Polyaniline, which can be attributed to the interactions between ferrite and Pani.

Lattice parameters (*a* and *c*) and crystallite size (*D*) of the substituted hexaferrites in Pani composites are obtained from Rietveld investigation and their values are listed in Table 1. It can be seen that the magnetic ferrites in the composites have kept the same volume cell and crystallite size as those of the hexaferrite alone [18]. The XRD analysis shows that Al^{3+}, Bi^{3+}, Cr^{3+} and Mn^{3+} ion are arranged within the hexagonal magnetoplumbite structure to maintain the formation of single phase which indicates

that the Solid-Based Polymerization preserves the crystalline characteristics of the magnetic particles [29, 30].

3.2. SEM for powder

SEM images of Pani and Pani/Ba*Me*$Fe_{11}O_{19}$ (*Me* = Al, Bi, Cr and Mn) prepared by Solid- Based Polymerization are shown in Fig. 2. The micrograph of Polyaniline reveals a uniform morphology with a rod-shaped particles with an average size of 1 ± 0.1 µm (Fig.2 a). These particles tend to form a connected network that favors the transport of electrons [31]. Fig. 2 (b - f) presents the SEM images of composites samples. As seen from these figures, the particles are agglomerated to form a cauliflower polymer composite where barium ferrite particles are encapsulated inside the Pani matrix. Here, with the Solid-Based method, Pani/Ba*Me*$Fe_{11}O_{19}$ powders can be obtained through a solventless medium without any organic phases and further surfactant contribution [32]. During polymerization, aniline in the presence ferrite particles reacts with APS to form the Polyaniline. Then, the growth of Pani continues on hexaferrite and favors the dispersion of the particles.

3.3. FTIR Spectra

Fig. 3 shows the FTIR spectra of pure Polyaniline and its composites obtained by Solid-Based Synthesis. The main wavenumber and assignments of the detected absorption bands are given in Table 2.

The characteristic peaks of Polyaniline are well observed, indicating the formation of Pani emeraldine salt [33]. These bands are assigned as follows:

The band at 1567 cm^{-1} can be mainly associated to the characteristic C=N stretching vibration of quinoid diimine unit N=Q=N, while the band near 1488 cm^{-1} is assigned to

the C-C aromatic ring stretching of benzenoid diamine unit N-B-N. The bands at 1297 and 1243 cm^{-1} correspond to π-electron delocalization induced in the polymer through protonation and asymmetric C-N-C stretching modes of benzenoid and $C-N^{+}$ stretching vibration of the polaron structure, respectively [34]. The wide band around 1125 cm^{-1} which is called conduction band, is attributed to the vibration mode of $B-NH^{+}=Q$ or $B-NH^{+}-B$ in the protoned emeraldine base form [35]. It refers to a clear delocalization of electrons in Pani [36]. The absorption band at 810 cm^{-1} corresponds to C-H out of plane vibration of the p-disubstituted benzene ring.

Compared to Pani FTIR spectrum (Table 2), the main absorption peaks observed for the composites and assigned above (Fig. 3) are shifted to higher wavenumber [37]. The relative oxidation level (Q/B) may be estimated from the ratio of quinoid and benzenoid band intensities [38]. These ratios are 0.86, 0.78, 0.84, 0.83, 0.84 and 0.82 for Pani, Pani/$BaFe_{12}O_{19}$, Pani/$BaAlFe_{11}O_{19}$, Pani/$BaBiFe_{11}O_{19}$, Pani/$BaCrFe_{11}O_{19}$ and Pani/$BaMnFe_{11}O_{19}$ samples, respectively. Polyaniline shows the highest oxidation ratio, which indicates the presence of more emeraldine salt form. This ratio decreases slightly with the addition of ferrite. Knowing that this ratio is related to the used oxidant and amount of H^{+} in the medium [39], the observed decrease may be due to the hydrogen bonding, between the hydrogen associated with amine groups in the Polyaniline backbone and the oxygen atom of the metal oxide in ferrite, thus, creating an electrostatic force between magnetic particles and the polymer [40].

In addition, Pani composites spectra indicate the presence of absorption bands in the range of 400 to 800 cm^{-1} which are a common feature of the hexaferrite (Table 2) [41]. The lower frequency absorption band ν_1 between 400 and 510 cm^{-1} is assigned to Fe-O bending vibration of octahedral site and the higher frequency absorption band ν_2 lying

in the range of 550 to 600 cm^{-1} is related to Fe-O stretching vibration in the tetrahedral site (Fig. 4) [42]. These absorption peaks blue shift compared to pure substituted hexaferrite. It can be explained by the fact that aniline initially is adsorbed in the surface of these magnetic particles [43]. When the APS is added, the polymerization process take place leading to the adhesion of the Pani on the hexaferrite particle to form these composites, as confirmed previously by the DRX study and SEM images.

3.4. TGA measurements

Among the key properties of polymer composites is their thermostability. It depends on the nature of the composite compounds, their interactions… Thermogravimetric curves of Pani composites are displayed in Fig. 5. All the samples present three major weight losses. Thermal degradation weight loss percentages for each composite are given in Table 4.

For Pani, a first weight loss of 9.2 % is observed up to 100 °C, which is most probably due to the evaporation of water and moisture. The second sharp weight loss in the range of 160 – 350 °C is attributed to the removal of the dopant anions bound to the polymer chain and degradation of oligomers. The slow and gradual third major loss above 430 °C is attributed to the complete decomposition of the Pani backbone [44, 45, 18].

Comparing with the thermal stability of Pani, the thermal behaviour of the Polyaniline/$BaFe_{12}O_{19}$ composite is found to increase. Initial weight loss of 5.5 % is observed up to 100 °C which may be associated to the loss of water molecules entrapped in the polymer matrix. From 220 to 380 °C, weight loss observed is 10 %, which is due to the partial leaching of the dopant from the polymer matrix. A weight loss of 38 % has been noted from 380 to 800 °C, which is attributed to the degradation of the polymer. This enhancement in the thermal stability can be due to the ionic

interactions of $BaFe_{12}O_{19}$ with amine group of aniline. These interactions limit the freedom of the polymer chains by improving the thermal degradation of this latter [18].

In other side, substituted ferrite composites exhibit greater thermal behaviour than Polyaniline. The composites synthesized hexaferrites substituted with small cations : Al^{3+} (ionic radius = 57 pm) and Cr^{3+} (ionic radius = 64 pm) have an improved thermal stability compared with Polyaniline/$BaFe_{12}O_{19}$ where Fe^{3+} having a radius of 67 pm (Table 3). In the case of iron substitution with cations whose ionic radius is larger than that of iron : Mn^{3+} (ionic radius = 70 pm), Bi^{3+} (ionic radius = 96 pm), one can see a smooth and gradual decline of TG curves and less weight losses than those of $BaAlFe_{11}O_{19}$ and $BaCrFe_{11}O_{19}$ (Table 4) [18]. This can be associated to the interactions between ferrite particles and the polymer matrix which are strongly influenced by lattice parameters of the ferrite [18].

3.5. Magnetic properties

Room temperature M–H hysteresis loops of Pani/Ba*Me*$Fe_{11}O_{19}$ composites (*Me* = Al, Bi, Cr and Mn) are shown in Fig. 6. The magnetization under applied magnetic field up to 1.8 T for all samples exhibits large hysteresis loops, demonstrating the ferromagnetic behaviour. The values of saturation magnetization (Ms), coercivity field (Hc), and the remnant magnetization (Mr) obtained from the curves are summarized in Table 4.

As listed in Table 4, saturations magnetization of Pani/$BaFe_{12}O_{19}$, Pani/$BaAlFe_{11}O_{19}$, Pani/$BaBiFe_{11}O_{19}$, Pani/$BaCrFe_{11}O_{19}$ and Pani/$BaMnFe_{11}O_{19}$ are 8.76, 7.82, 6.46, 7.39 and 8.32 $Am^2.\ kg^{-1}$, respectively. In addition, their coercivity increased compared to pure substituted ferrite.

According to the physical point of view, the magnetic properties of a material are related to the magnetic polarization J proportional to the magnetization [46]. Generally, the measuring methods to determinate the magnetic properties of the sample are in terms of moment per unit mass (M). So, the magnetic polarization is written following the relation

$$J = \mu_0 \rho M \qquad (1)$$

with μ_0 is the magnetic permeability of the vacuum with numerical value $4 \pi 10^{-7}$ H. m^{-1} and ρ is the volumic mass of the sample.

In case of a composite formed by a mixture of two phases, J depends on the volume fraction and the magnetic polarization of each phase. For Polyaniline/hexaferrite, the magnetic polarization of the composite J_C may be expressed as

$$J_C = Ø_{HF} J_{HF} + (1- Ø_{HF}) J_P \qquad (2)$$

with $Ø_{HF}$ and J_{HF} are the volume fraction and the magnetic polarization of hexaferrite, respectively, and J_P is the magnetic polarization of Pani.

As reported in the literature, the magnetic polarization is strongly dependent to the real particles loading in the formed composite. Actually, the used initial loading to prepare the samples can change after the polymerizations synthesis due to partial loss or dissolution during the fabrication as we have demonstrated in our previous study [18]. Considering that, real weight fraction w_{rHF} of the samples are determined by using measured M_s in Table 4 as follow :

$$w_{rHF} = \frac{M_{sC}}{M_{sHF}} \qquad (3)$$

Where M_{sC} and M_{sHF} are the magnetization saturation of the composite and hexaferrite, respectively.

The volume fraction is deduced using the real weight fraction w_{rHF} of hexaferrite in the composites and the volumic mass of the corresponding hexaferrite and Polyaniline by the following equation:

$$\emptyset_{HF} = \frac{\rho_C}{\rho_{HF}} \; w_{rHF} \qquad (4)$$

To determine the hexaferrites loading in the composites theoretical and real weight fractions are used:

$$\text{Loading} = \frac{w_{rHF}}{w_{tHF}} \times 100 \qquad (5)$$

The calculated values of real weight fraction and the loading of ferrites in the composites are presented in Table 5. Thus, the real weight fraction of hexaferrite in the composites is about 14 ± 1 % close to that theoretical one (16.4%) with global loading between 80 and 90 %. These results are explained by a lower loss of ferrite particles during formation of composites in a solventless medium [18].

The coercivity values of composites increased slightly in comparison to substituted ferrite as observed in Table 5. The increase in Hc can be explained by the pinning of the domain walls. It can be due to the Pani matrix that precluded the movement of the latter causing the increase of Hc in the composites. In fact, an interfacial effect between ferrite particles and Pani surface layers may exert an additional resistance for the alignment of magnetic moment during the magnetization process under the external applied magnetic field [47].

3.6.Complex permittivity and permeability microwave spectrometry

In this subsection, we briefly discuss the method for measuring the complex permittivity (ε^*) and permeability (μ^*) which are a special relevance to isotopic materials in the

microwave region of the electromagnetic spectrum. The effective complex permittivity $\varepsilon^* = \varepsilon' - j\,\varepsilon''$ and permeability $\mu^* = \mu' - j\,\mu''$ of the composite samples are measured using the Transmission/Reflection (T/R) method based on the Nicolson and Ross [48, 49], Weir [50], and Baker-Jarvis and al. [51, 52] algorithms for the characterization of isotropic solid materials. This experimental technique is based on the measurement of the scattering parameters (S parameters) of a toroidal (or rectangular) sample of the test material which is machined in order that the geometrical dimensions fit well those of the used coaxial line (or rectangular waveguide) to avoid the presence air gaps between the sample and the line walls. The geometry of the cell, including the sample of the material to be tested, is illustrated in Fig. 7 a.

The method enables to calculate simultaneously the permittivity and the permeability of the material from the measurement of the transmission S_{21} and reflection S_{11} parameters, i.e. Fig. 7 b, of a coaxial line that contains it. The electromagnetic analysis of the propagation line allows us to write:

$$S_{21}(\omega) = \frac{(1-\Gamma^2)\,T^2}{1-\Gamma^2\,T^2} \tag{6}$$

$$S_{11}(\omega) = \frac{(1-T^2)\,\Gamma^2}{1-\Gamma^2\,T^2} \tag{7}$$

Where Γ is the reflection coefficient at the interface between the air-filled transmission line and dielectric and permeability-filled line when the length of materials is infinite, and T denotes the transmission coefficient in the material (of finite length).

Equation (6) and equation (7) allow Γ and T to be derived by measuring $S_{11}(\omega)$ and $S_{21}(\omega)$. These values can then be used to calculate μ^* and ε^* as follows:

$$\mu^* = \mu' - j\,\mu'' = \frac{(1+\Gamma)}{(1-\Gamma)}\,\frac{j\ln(T)}{2\,\pi\,d}\,\frac{c}{F} \tag{8}$$

$$\varepsilon^* = \varepsilon' - j\,\varepsilon'' = \frac{\left(\frac{J\ln(T)}{2\,\pi\,d}\,\frac{c}{F}\right)}{\mu^*} \tag{9}$$

Where c denotes the velocity of light in free space, d is the thickness of the material sample and $f = \omega/2\pi$ is the frequency of the wave, respectively.

In this coaxial line, the measurement uses the fundamental transverse electromagnetic TEM mode, which is the only mode that propagates in the coaxial line. The dimension of the sample is adapted to the internal (3.04 mm) and external (7 mm) diameter of the coaxial line (Z_0 = 50 Ω). An error analysis indicates modest uncertainties in ε ´and μ´ (< 5%) for the data. An Agilent N6230A network analyzer setup is used to S parameters measurement of the cell containing the material sample under test over a wide range of frequencies (100 MHz – 18 GHz) (Fig. 8). We apply the Short-Open-Load and Thru (SOLT) calibration to the measurement since this method permits error correction over a wide frequency band.

Fig. 9 shows the variation of the real (ε´) and imaginary (ε´´) parts of complex permittivity and the real (μ´) and imaginary (μ´´) parts the complex permeability for the Pani and Pani/Ba*Me*$Fe_{11}O_{19}$ (*Me*$^{3+}$ = Al^{3+}, Bi^{3+}, Cr^{3+} and Mn^{3+}) composites in the frequency range of 100 MHz to 18 GHz.

As shown in Fig. 9 a, the real part ε´ spectra of all samples display an almost constant value over the frequency range from 100 MHz to 4 GHz which increases rapidly with increasing frequency up to 18 GHz. The ε´spectrum for Pani is the lowest and its values lay from 7.4 at 100 MHz to 7.6 at 3 GHz, with an almost constant behaviour. Then a resonance peak at 3 GHz is observed. The real ε´ spectrum for Pani/$BaFe_{12}O_{19}$

composite shows the highest values from 8.1 at 100 MHz to 7.9 at 4.5 GHz, a decreasing trend with increasing frequency, meanwhile, the spectra of ε′ for the other composites are between those Pani and Pani/$BaFe_{12}O_{19}$ with a decreasing trend. The resonance behaviour observed previously for Pani shifts to a higher frequency for the composites at 6 GHz. This shift is due to the heterogeneity of the material as ferrite particles are imbibed in the Polyaniline matrix. In particular, it is associated to the orientation polarization mechanism sustained by the presence of relaxation behaviour in the ε′′ plot [53].

In other hand, the dielectric loss ε′′ presents an increasing trend towards high frequencies (Fig. 9 b). The ε′′ spectrum of Polyaniline shows a resonance peak with a value of 1.2 at 4.5 GHz, which, decreases for the composites to 0.4 at 5.6 GHz. At room temperature, the conducting Polyaniline in its emeraldine salt form possesses permanent electric dipoles which give rise to permanent electric dipoles. Therefore, orientation polarization is the dominant polarization and the resulting relaxation behaviour constitutes the loss mechanism [54]. In addition, the phenomena of polarization in Pani/hexaferrite can be attributed to presence of Ba^{2+} and Fe^{3+} cations at their respective position in the crystallographic lattice in $BaFe_{12}O_{19}$ They form an electric dipole with the surrounding O^{2-} ions contributing to the real part ε′ evolution through dipolar polarization and to the imaginary part ε′′ by dipole relaxation [55]. In the case of substituted hexaferrite, the ions substitution of Fe^{3+} by diverse trivalent ion Me^{3+} with different valence leads to a different coordination with O^{2-} ions, to form dipoles with modified strength. These dipoles contribute to decrease ε′ and ε′′. So, the behaviour of complex permittivity towards composition changes, takes place by means of a

mechanism similar to the conduction process by electron exchange in ferrite causing electric polarization.

Fig. 9 c and d show the spectra of real (μ´) and the imaginary (μ´´) parts of the complex permeability for the Polyaniline composites. It is worth noting that the plots of μ´ present a gradual decrease with increasing frequency for all the composites (Fig. 9 c), meanwhile, those of μ´´ show a large resonance loss peak at high-frequency regions (Fig. 9 d). The values of the real (μ´) decreased from 1 and 0 in the whole frequency range for the different samples. Those of the imaginary (μ´´) are around 0.4 and 0. As expected, the permeability of the composites is higher than that of Polyaniline alone. And the resonance frequencies have moved to higher frequencies. In fact, the effect of incorporating the hexaferrite into the polymer matrix increases the real part μ´ above unity at low frequencies and lowers μ´ at high frequencies. At the same time, it increases the imaginary part μ´´ above zero through the whole frequency range. A closer look at the logarithmic plot indicates a resonance peak at approximately 3.5 GHz. This peak can be attributed to the interaction of magnetic material and conducting polymer. Pani exhibits a low wall resonance due to its paramagnetic properties, the addition of ferromagnetic ferrite contributed to the variation of the permittivity in the composites. On the other hand, this behaviour is due to a possible charge transfer between the ferrite surface and the Polymer. This latter may change the electron density at the ferrite surface and thus affect magnetic relaxation processes in the system [56].

Besides, it is known that the resonance frequency mainly depends of the microscopic demagnetizing fields in the composite which is associated to the modifications of the dipolar interactions and the particles arrangement of the ferromagnetic fillers [57]. In our composite materials, the resonance frequency f_r can be given by the relation [58]:

$$f_r = \left(\frac{\gamma}{2\pi}\right)(H_a + H_d) \quad (10)$$

$$H_a = \left(\frac{2}{3}\frac{2\,K_1}{\mu_0\,M_s}\right) \quad (11)$$

Where γ the gyromagnetic ratio, H_a the magnetic-field anisotropy and H_d the demagnetizing field. The latter quantity is strongly affected by the structural disorder in the ferrite, by both the crystallographic and the geometrical structure.

Generally, $BaFe_{12}O_{19}$ with its large anisotropic field exhibits a ferromagnetic resonance peak at 47.6 GHz [59]. Besides to the contribution of Pani, this resonance peak can be shifted to any frequency region due to the Fe^{3+} substitution [60]. In the present polymer ferrite compositions, the substitution of iron by trivalent ion lowers the magnetic field anisotropy and influences the spin rotation resonance in composite materials. The Pani composites display great dielectric loss and magnetic loss which may be candidates for broadband and highly efficient microwave absorbing materials.

The reflexion loss (RL, dB) plotting as a function of frequency in the range of 1 - 18 GHz for pure Pani and its composites are given in Fig. 10. Measured values of ε´, ε´´, μ´ and μ´´ (Fig. 9) are used to determine RL of the electromagnetic radiation under normal wave incidence in the composite samples based on a model of single-layered lane wave absorber [61]. RL is calculated using the transmission line theory based on the complex permittivity and permeability of the sample as:

$$RL\ (dB) = 20\log\left|\frac{Z_{in} - Z_0}{Z_{in} + Z_0}\right| \quad (12)$$

where Z_{in} is the input impedance at the materials interface and the free space:

$$Z_{in} = Z_0 \sqrt{\frac{\mu^*}{\varepsilon^*}} \tanh\left[j \frac{2\,\pi\, f\, d}{c} \sqrt{\mu^*\, \varepsilon^*} \right] \quad (13)$$

and Z_0 is the characteristic impedance of the free space:

$$Z_0 = \sqrt{\frac{\mu_0}{\varepsilon_0}} \quad (14)$$

where μ^* and ε^* the complex permeability and complex permittivity of the composite absorber, respectively, c the velocity of light in free space, *f* the frequency and d the thickness of the sample. The reflexion loss is calculated from computer simulation using equations (12) and (13) for various values of complex permittivity and permeability of the samples.

Fig. 10 a shows eight reflection dips for pristine Polyaniline which appeared in Ku-band and X-band. Their bandwidth increased with decreasing thickness of the material from 10.97 GHz to 16.02 GHz. For barium hexaferrite composite, two absorption peaks can be seen at a frequency of 14.14 GHz and 16.25 GHz with reflexion losses of -101.46 dB and -93.94 dB, respectively (Fig. 10 b). This behaviour can be attributed to domain wall resonance and natural ferromagnetic resonance in the hexaferrite [62].

As shown in Fig. 10 c - f, the substituted hexaferrite composites have one maximum absorption peak with an RL of -101.12, -88.31, -80.58 and -91.81 dB for Pani/$BaAlFe_{11}O_{19,}$ Pani/$BaBiFe_{11}O_{19}$, Pani/$BaCrFe_{11}O_{19}$ and Pani/$BaMnFe_{11}O_{19}$, respectively. Their resonance frequency corresponding to the maximum reflexion peak (f_r) are 16.05, 14.14, 16.23, 15.70 GHz, associated to the calculated matching thickness is 20, 25, 27, 31 and 29 mm, respectively. The presence of this major reflexion loss is due to iron Fe^{3+} substitution with trivalent ion with lower magnetic moment into to barium hexaferrite structure modifying the magneto-crystalline anisotropy of the

material along c-axis [63]. As a result, the anisotropy constant decreased and the reflection dip frequency is located at Ku-band range based on the equations (8) and (9). Knowing that this anisotropy is the effective coupling of the spins of the magnetic ions and the crystalline electric fields influencing the ions via spin-orbit coupling, with such substitutions the resonance frequency can be shifted to lower frequency [64].

The evolution of the bandwidth (reflection loss > - 20 dB) of Polyaniline composites is presented in Fig. 11. The absolute value of RL higher than 20 dB means that the material absorbs 99% of the input power. It is observed that reflexion loss values for all the samples are above 40 dB. These results can be related to promising shielding properties. The samples show excellent absorption properties in a relatively wide bandwidth in the frequency region from 8 GHz to 18 GHz. The bandwidth plot of Pani/$BaFe_{12}O_{19}$ spreads the Ku-band, meanwhile, it expands to X-band for the substituted composites. The tendency of the microwave absorption properties after Fe^{3+} substitution may be ascribed to the follow changes: the distribution, the magnetic moment, the exchange of ions and the magneto-crystalline anisotropy changes after the trivalent ion entering the lattices of barium hexaferrite [63]. In fact, $BaFe_{12}O_{19}$ is an M-type hexaferrite, and its Fe^{3+} is located in the center of the oxygen in three octahedral sites and one tetrahedral site and one bipyramidal site. The properties of this ferrite arise from exchange interactions between the oxygen and metallic ions occupying particular positions in its hexagonal crystalline structure. In case of magnetic ion substitution by Cr^{3+} and Mn^{3+}, the magnetic properties are not altered because both have the same magnetic moment as Fe^{3+}. For non-magnetic Al^{3+} and Bi^{3+} doping will reduce the whole magnetic properties of barium ferrite because they have low magnetic moments. So, the

ferromagnetic resonance frequency varies, resulting in the variation of microwave absorption properties.

Furthermore, the coating of hexaferrite by the polymer increased the complex permittivity. So, dielectric loss becomes the main absorbing mechanism of the composite in low frequency, and the electromagnetic waves are absorbed drastically in X-band as shown in Fig. 11 [65]. These two factors together (substitution and coating) result in a shift of the microwave absorption properties of Pani/$BaFe_{12}O_{19}$ composite to the low frequencies from the Ku band to the X-band for substituted hexaferrite's composites.

4. Conclusion

Polyaniline/Ba*Me*$Fe_{11}O_{19}$ (*Me* is an element in a trivalent state; *Me* = Al, Bi, Cr and Mn) composites with 10 % volume fraction are successfully obtained by Solid-Based Polymerization then the influence of iron substitution in hexaferrite's composites is studied. XRD confirms that Al^{3+}, Bi^{3+}, Cr^{3+} and Mn^{3+} ions are arranged within the hexagonal magnetoplumbite structure to maintain the formation of a single phase of ferrite which shows that the Solid-Based Polymerization preserves the crystalline characteristics of the magnetic particles. The results of the FTIR analysis reveal that there are interactions among Pani matrix and hexaferrite particles. SEM images clearly show that solid-based polymerization (solventless medium) reveals a less agglomerated particles with cauliflower morphology due to a strong interaction between hexaferrite and Pani. The thermal stability of composite Pani/$BaFe_{12}O_{19}$ increases when small ions, (Al^{3+} and Cr^{3+}) substituted Fe^{3+} in hexaferrite compared with large cations substitution (Bi^{3+} and Mn^{3+}). The magnetic properties determined by VSM indicate that all

composites exhibit a clear hysteretic behaviour. Magnetization saturation Ms is found to be related to the ferrite weight fraction. However, there is an increase of coercivity field compared to that of pure hexaferrite due to the Pani matrix that precluded the movement of ferrite domain walls. The complex permittivity ε^*, permeability μ^* and their relationship with microwave absorption properties are then investigated in the 100 MHz - 18 GHz microwave frequency range. Pani/$BaFe_{12}O_{19}$ shows the highest complex permittivity compared to the substituted hexaferrite composites. Its resonance peak shifts to higher frequencies from 4.5 GHz to 5.6 GHz. In other hand, the permeability of the Polyaniline/Ba$Me_xFe_{12-x}O_{19}$ is greater than that of Polyaniline and manifests a large resonance loss peak at 3.5 GHz. Different mechanisms can contribute to changes in the permittivity and permeability of the composites upon the addition of ferrite particles in the conductive polymer. In fact, such variations are due to the formation of dipoles between iron substituting ion and surrounding O^{2-} in the ferrite that are responsible for ferromagnetic resonance and magneto-crystalline anisotropy and to exchange interaction with the polymer. In addition, it may be associated to the pinning of surface domain walls that are formed by Pani chains growing on the surface of a ferrite particles. Measured values of ε^* and μ^* are used to determine RL of the electromagnetic radiation under normal wave incidence in the composite samples. The Pani/$BaFe_{12}O_{19}$ powder shows better absorption bands than substituted hexaferrite polymer composites at the X-band. On the other side, among the 1 - 18 GHz range, the maximum reflexion loss band for the substituted hexaferrite samples (below -20 dB) reaches Ku band. This shift in microwave-absorbing properties is due to the substitution in ferrite and to Pani coating. This in turn focuses the importance of substituted ferrite

composites as their RL values are above 40 dB, they can be considered as microwave absorbers.

Acknowledgements

Authors are thankful to Université de Tunis El Manar, Tunis for the financial support to achieve this work and grateful for the funding obtained in the framework of scholarship for international students at SATIE, ENS de Cachan for 12 months.

References

[1] V.M. Petrov, V.V. Gagulin, Microwave absorbing materials, Inorg. Mater. 37, (2001) 93-98.

[2] D. Yan, S. Cheng, R.F. Zhuo, J.T. Chen, J.J. Feng, H.T. Feng, Nanoparticles and 3D sponge-like porous networks of manganese oxides and their microwave, absorption properties, Nanotechnol 20 (2009) 105706-105716.

[3] N. Zhao, T. Zou, C. Shi, J. Li, W. Guo, Microwave absorbing properties of activated carbon-fiber felt screens (vertical-arranged carbon fibers)/epoxy resin composites, Mater. Sci. Eng. B 127 (2006) 207-211.

[4] N. Chen, K. Yang, M.Y. Gu, Microwave absorption properties of La-substituted M-type strontium ferrites, J. Alloys Compd. 490 (2010) 609-612.

[5] J. Zhao, Y. Xie, C. Yu, Z. Le, R. Zhong, Y. Qin, J. Pan, F. Liu, Preparation and characterization of the graphene-carbon nanotube / CoFe2O4/ polyaniline composite with reticular branch structures, Mater. Chem. Phys. 123 (2013) 395-402.

[6] G. Liu, L.Y. Wang, G.M. Chen, S.C. Hua, C.Q. Ge, H. Zhang, R.B. Wu, Enhanced electromagnetic absorption properties of carbon nanotubes and zinc oxide whisker microwave absorber, J. Alloys Compd. 514 (2012) 183-188.

[7] W.C. Zhou, X.J. Hu, X.X. Bai, S.Y. Zhou, C.H. Sun, J. Yan, P. Chen, Synthesis and electromagnetic, microwave absorbing properties of core-shell Fe_3O_4-Poly(3, 4-ethylene dioxythiophene) microspheres, ACS Appl. Mater. Interfaces 3 (2011) 3839-3845.

[8] K.Y. Chen, C. Xiang, L.C. Li, H.S. Qian, Q.S. Xiao, F. Xu, A novel ternary composite: fabrication, performance and application of expanded graphite/polyaniline/$CoFe_2O_4$ ferrite, J. Mater. Chem. 22 (2012) 6449-6455.

[9] P. Xu, X. Han, J. Jiang, X. Wang, X. Li, A. Wen, Synthesis and characterization of novel coralloid polyaniline/$BaFe_{12}O_{19}$ nanocomposites, J. Phys. Chem. C 111 34 (2007) 12603-12608.

[10] C.C. Yang, Y.J. Gung, W.C. Hung, T.H. Ting, K.H. Wu, Infrared and microwave absorbing properties of $BaTiO_3$/polyaniline and $BaFe_{12}O_{19}$ / polyaniline composites, Compos. Sci. and Technpl. 70 (2010) 466-471.

[11] L. Du, Y. Du, Y. Li, J. Wang, C. Wang, X. Wang, P. Xu, X. Han, Surfactant-assisted solvothermal synthesis of $Ba(CoTi)_xFe_{12-2x}O_{19}$ nanoparticles and enhancement in microwave absorption properties of polyaniline, J. Phys. Chem. C 114(2010) 19600-19606.

[12] P. Zhang, X.J. Han, L.L. Kang, R. Qiang, W.W. Liu, Y.C. Du, Synthesis and characterization of polyaniline nanoparticles with enhanced microwave absorption, RSC Adv. 3 (2013) 12694-12701.

[13] N.A. Spaldin, Magnetic materials fundamentals and applications, second ed., University Press, Cambridge, The Edinburgh Building (2010).

[14] P. Xu, X. Han, J. Jiang, X. Wang, X. Li, A. Wen, Synthesis and characterization of novel coralloid polyaniline/$BaFe_{12}O_{19}$ nanocomposites, J. Phys. Chem. C111 34 (2007) 12603-12608.

[15] J. Jiang, L.H. Ai, D.B. Qin, H. Liu, L.C. Li, Preparation and characterization of electromagnetic functionalized polyaniline/$BaFe_{12}O_{19}$ composites, Synth; Met. 159 (2009) 695-699

[16] T. Ting, K. Wu, Synthesis, characterization of polyaniline/$BaFe_{12}O_{19}$ composites with microwave-absorbing properties, J. Magn. Magn Mater. 322 (2010) 2160-2166

[17] S.N. Ezzatia, M. Rabbani, R.M. Leblanc, E. Asadi, S.M.H. Ezzati, R. Rahimi, S. Azodi-Deilami Conducting, magnetic polyaniline/$Ba_{0.25}Sr_{0.75}Fe_{11}(Ni_{0.5}Mn_{0.5})O_{19}$ nanocomposite: fabrication, characterization and application, J. Alloys Compd. 646, (2015) 1157-1164.

[18] T.B. Ghzaiel, W. Dhaoui, A. Pasko, F. Mazaleyrat, Optimization of multiroute synthesis for polyaniline-barium ferrite composites, Mater. Chem. and phys. 179 (2016) 42-54.

[19] L.A. Bashkirov, Y.L. Kostyushko, Formation of ferrite-chromites $BaFe_{10}Cr_2O_{19}$ and $SrFe_{10}Cr_2O_{19}$ in the solid-phase reaction of Fe_2O_3 and Cr_2O_3 with barium or strontium carbonate, Russ. J. Appl. Chem. 78 (2005) 351-355.

[20] Y. Liu, M.G.B. Drew, J. Wang, M. Zhang, Y. Liu, Efficiency and purity control in the preparation of pure and/or aluminum-doped barium ferrites by hydrothermal methods using ferrous ions as reactants, J. Magn. Magn. Mater. 322 (2010) 366-374.

[21] S.N. Ezzatia, M. Rabbani, R.M. Leblanc, E. Asadi, S.M.H. Ezzati, R. Rahimi, S. Azodi-Deilami Conducting, magnetic polyaniline/$Ba_{0.25}Sr_{0.75}Fe_{11}(Ni_{0.5}Mn_{0.5})O_{19}$ nanocomposite: fabrication, characterization and application, J. Alloys Compd. 646, (2015) 1157-1164.

[22] A. Tadjarodi, H. Kerdari, M. Imani, $Ba_{0.69}Sr_{0.17}Cd_{0.07}Zn_{0.07}Fe_{12}O_{19}$ nanostrucutres / conducting polyaniline nanocomposites; synthesis, characterization and microwave absorption performance, J. Alloys Compd. 554 (2013) 284-292.

[23] T.B. Ghzaiel, W. Dhaoui, A. Pasko, F. Mazaleyrat, Effect of non-magnetic and magnetic trivalent ion substitutions on BaM-Ferrite properties synthesized by hydrothermal method, Alloys Compd. 671 (2016) 245-253.

[24] H. M. Rietveld, A profile refinement method for nuclear and magnetic structures, J. Appl. Cryst. 2 (1969) 65-71.

[25] M. Ferrari, L. Lutterotti, Method for the simultaneous determination of anisotropic residual stresses and texture by X-ray diffraction, J. Appl. Phys. 76 (1994) 7246-7255.

[26] J. Baker-Jarvis, M.D. Janezic, Jr. J.H. Grosvenor, R.G. Geyer, Transmission/Reflection and short-circuit line methods for measuring permittivity and permeability, NIST Technical Note 1355 (revised), National Institute of Standards and Technology, Boulder, Co, (1993).

[27] M.E. Jozefowicz, R. Laversanne, H.S. Javadi, A.J. Epstein, J. P. Pouget, X. Tang, A.G. MacDiarmid, Multiple lattice phases and polaron-lattice-spinless-defect competition in polyaniline, Phys. Rev B39 (1989) 12958-12961.

[28] J.P. Pouget, M.E. Jozefowicz, A.J. Epstein, X. Tang, A.G. MacDiarmid, X-ray structure of polyaniline, macromolecules 24 (1991) 779-789.

[29] M. Rosler, P. Girmert, E. Sinn, Structural and magnetic of Ba-ferrite fine particles grown by glass crystallization, Z. Phys. D Atom. Mol. CL 19 (1991) 279-281.

[30] M.A. Blesa, P.J. Morando, A.E. Regazzoni, Chemical dissolution of metal oxides, CRC Press, Boca Raton, (1994).

[31] Y. Li, H. Zhang, Y. Liu, Q. Wen, J. Li, Rod-shaped polyaniline–barium ferrite nanocomposite: preparation, characterization and properties, Nanotechnology, 19 (2008) 105605-105610.

[32] I. Sapurina, A. Riede, J. Stejskal, In-situ polymerized polyaniline films: 3. Film formation, Synth. Met. 123 (2001) 503-507.

[33] A. Wolter, P. Rannou, J.P. Travers, Model for aging in HCl-protonated polyaniline: structure, conductivity, and composition studies, Phys. Rev. B 58 (1998) 7637-7647.

[34] J. Stejskal, I. Sapurima, J. Prokes, J. Zemek, In-situ polymerized polyaniline films, Synth. Met. 105 (1999) 195-202.

[35] E.N. Konyushenko, J. Stejskal, I. Sedenkova, I. Sapurina, M. Cieslar, J. Prokes, Polyaniline nanotubes: conditions of formation, Polym. Int. 55 (2006) 31-39.

[36] U.S. Sajeev, C.J. Mathai, S. Saravanan, R.R. Ashokan, S. Venkatachalam, M.R. Anantharaman, On the optical and electrical properties of rf and ac. plasma polymerized aniline thin films, Bull. Mater. Sci. 29 (2006) 159-163.

[37] V.M. Mzenda, S.A. Goodman, F.D. Auret, L.C. Prinsloo, Characterization of electrical charge transfer in conducting polyaniline over the temperature range 300 < T (K) < 450, Synth. Met. 127 (2002) 279-283.

[38] N. Gospodinova, L. Trlemezyan, Conducting polymers prepared by oxidative polymerization: pol8yaniline, Prog. Polym. Sci. 23 (1998) 1443-1484.

[39] W. Shao, R. Jamal, F. Xu, A. Ubul, T. Abdiryim, The effect of a small amount of water on the structure and electrochemical properties of solid-State synthesized polyaniline, Materials 5 (2012) 1811-1825.

[40] W. Wang, S.P. Gumfekar, Q. Jiao, B. Zhao, Ferrite-grafted polyaniline nanofibers as electromagnetic shielding materials, J. Mater. Chem. C 1 (2013) 2851-2859.

[41] F.M.M. Pereira, C.A.R Junior, M.R.P. Santos, R.S.T.M. Sohn, F.N.A. Freire, J.M. Sasaki, J.A.C. De Paiva, A.S.B. Sombra, Structural and dielectric spectroscopy studies of the M-type barium strontium hexaferrite alloys ($Ba_xSr_{1-x}Fe_{12}O_{19}$), J. Mater. Sci. Mater. Electron. 19 (2008) 627-638.

[42] Z. Mosleh, P. Kamelin , M. Ranjbar, H. Salamati, Effect of annealing temperature on structural and magnetic properties of $BaFe_{12}O_{19}$ hexaferrite nanoparticles, Ceram. Int. 40 (2014) 7279-7284.

[43] E.N. Konyushenko, J. Stejskal, M. Trchova, J. Hradil, J. Kovarova, J. Prokes, M. Cieslar, J.Y. Hwang, K.H. Chen, I. Sapurina, Multi-wall carbon nanotubes coated with polyaniline, Polymer 47 (2006) 5715-5723.

[44] W. Dhaoui, S. Hbaieb, H. Zarrouk, A.B. Mohamed, Investigation of spectral properties, thermal stability, and morphology in polyaniline doped with chlorocarboxylic acids, Int. J. Polym. Anal. Charact. 11 (2006) 239-252.

[45] S. Bhadra, D. Khastgir, Extrinsic and intrinsic structural change during heat treatment of polyaniline, Polym. Degrad. Stab. 93 (2008) 1094-1099.

[46] B. D. Cullity, C. D. Graham, Introduction to magnetic materials, second ed., Wiley-IEEE Press, (2008).

[47] M. Asghari, A. Ghasemi, E. Paimozd, A. Morisako, Evaluation of microwave and magnetic properties of substituted $SrFe_{12}O_{19}$ and substituted $SrFe_{12}O_{19}$/multi-walled carbon nanotubes nanocomposites, Mater. Chem. Phys. 143 (2013) 161-166.

[48] A.M. Nicolson, G.F. Ross, Measurement of the intrinsic properties of materials by time-domain techniques, IEEE Trans. Instrum. Meas., 19 (1970) 377-383.

[49] A.M. Nicolson, Broad-band microwave transmission characterization from a single measurement of the transient response, IEEE Trans. Instrum. Meas., 17, (1968), 395-402.

[50] W.B. Weir, Automatic measurements of complex dielectric constant and permeability at microwaves frequencies, Proc. IEEE Trans. Instrum. Meas., 62, (1974), 33-39.

[51] J. Baker-Jarvis, M.D. Janezic, J.H. Jr. Grosvenor, R.G. Geyer, Transmission/Reflection and short-circuit line method for measuring permittivity and permeability, Nat. Inst. Stand Tech. Tech. Note 1355-R, (1993).

[52] J. Baker-Jarvis, E.J. Vanzura, W.A. Kissick, Improved technique for determining complex permittivity with Transmission/Reflection method, IEEE Trans. on Microwave Theory and Techniques, 38 (1990) 1096-1102.

[53] J. Jacob, L.H.L. Chia and F. C.Y. Boey, Thermal and non-thermal interaction of microwave radiation with materials, J. Mater. Sci. 30 (1995) 5231- 5327.

[54] S.M. Abbas, A.K. Dixit, R. Chatterjee, T.C. Goel, Complex permittivity and microwave absorption properties of $BaTiO_3$–polyaniline composite, Materials Science and Engineering B 123 (2005) 167-171.

[55] J. Sobhanadri, R. Raman, Ferrite Materials: Science and technology, edited by B. Viswanathan and V. R. K. Murthy Narosa, New Delhi, (1990).

[56] M. Fahlman, S. Jasty, A.J. Epstein, Corrosion protection of iron/steel by emeraldine base polyaniline: an X-ray photoelectron spectroscopy study, Synth. Met. 85 (1997) 1323-1326.

[57] A. Chevalier, M. Le Floc'h, Dynamic permeability in soft magnetic composite materials, Appl. Phys. 90 (2001) 3462-3465.

[58] J.L. Snoek, Dispersion and absorption in magnetic ferrites at frequencies above one Mc/s, Physica 14 (1948) 207-217.

[59] B. Zhang, Y. Du, P. Zhang, H. Zhao, L. Kang, X. Han, P. Xu, Microwave absorption enhancement of Fe_3O_4/polyaniline core/shell hybrid microspheres with controlled shell thickness, J. Appl. Polym. Sci. 130 (2013) 1909-1916.

[60] P. Xu, X. Han, J. Jiang, X. Wang, X. Li, A. Wen, Synthesis and characterization of novel coralloid polyaniline/$BaFe_{12}O_{19}$ nanocomposites, J. Phys. Chem. C 111 (2007) 12603-12608.

[61] Y. Naito, K. Suetake, Application of ferrite to electromagnetic wave absorber and its characteristics, IEEE Trans. Microwave Theory Tech. 19 (1971) 65-72.

[62] A. Ghasemi, X. Liu, A. Morisako, S.E. Shirsath, Magnetic and reflection loss characteristics of $SrFe_{12-x}(Sm_{0.5}Dy_{0.5})_xO_{19}$/multiwalled carbon nanotube nanocomposite, IEEE Trans. Magn. 49 (2013) 4218-4221.

[63] A. Ghasemi, S. E. Shirsath, X. Liu and A. Morisako, A comparison between magnetic and reflection loss characteristics of substituted strontium ferrite and nanocomposites of ferrite/carbon nanotubes, J. Appl. Phys. 111 (2012) 07B543-1-3.

[64] Z. De-Xu, L. Qiao-Ling, Y. Yun and Z. Cun-rui, Synthesis and characterization of carbon nanotubes decorated with strontium ferrite nanoparticles, J. Synth. Met. 160 (2010) 866-870.

[65] J. Liu, J. Zhang, Y. Li, M. Zhang, Microwave absorbing properties of barium hexa-ferrite/polyaniline core-shell nano-composites with controlled shell thickness, Mater. Chem. Phys. 163 (2015) 470-477.

Figures Captions

Fig. 1. XRD patterns of (a) Pani, (b) Pani/$BaFe_{12}O_{19}$, (c) Pani/$BaAlFe_{11}O_{19}$, (d) Pani/$BaBiFe_{11}O_{19}$, (e) Pani/$BaCrFe_{11}O_{19}$ and (f) Pani/$BaMnFe_{11}O_{19}$

Fig. 2 SEM images of (a) Pani, (b) Pani/$BaFe_{12}O_{19}$, (c) Pani/$BaAlFe_{11}O_{19}$, (d) Pani/$BaBiFe_{11}O_{19}$, (e) Pani/$BaCrFe_{11}O_{19}$ and (f) Pani/$BaMnFe_{11}O_{19}$

Fig. 3. FTIR absorption spectra of Pani and Pani/ Ba*Me*$Fe_{11}O_{19}$ composites

Fig. 4. Zoom scanning of the FTIR spectra for the vibrations regions related to Fe-O group

Fig. 5. TG curves of Pani and Pani/Ba*Me*$Fe_{11}O_{19}$ composites

Fig. 6. Magnetic hysteresis loops for Pani/Ba*Me*$Fe_{11}O_{19}$ composites at room temperature.

Fig. 7. Principle of measurement of the effective permittivity and permeability of toroidal material sample: a) a schematic diagram of the experimental setup showing its different parts and b) measurement of the S parameters. The thickness of the material sample having effective (relative) permittivity ε^* and permeability μ^* is d

Fig. 8. Experimental device for the measurement of the scattering parameters (S21 and S11) vs frequency of the transmission coaxial loaded by composite toroidal samples.

Fig. 9. Complex permittivity and permeability of Pani composites

Fig. 10. The reflexion loss curves of (a) Pani, (b) Pani/$BaFe_{12}O_{19}$, (c) Pani/$BaAlFe_{11}O_{19}$, (d) Pani/$BaBiFe_{11}O_{19}$, (e) Pani/$BaCrFe_{11}O_{19}$ and (f) Pani/$BaMnFe_{11}O_{19}$

Fig. 11. Evolution of the bandwidth of different composites as function of thickness

Fig. 1.

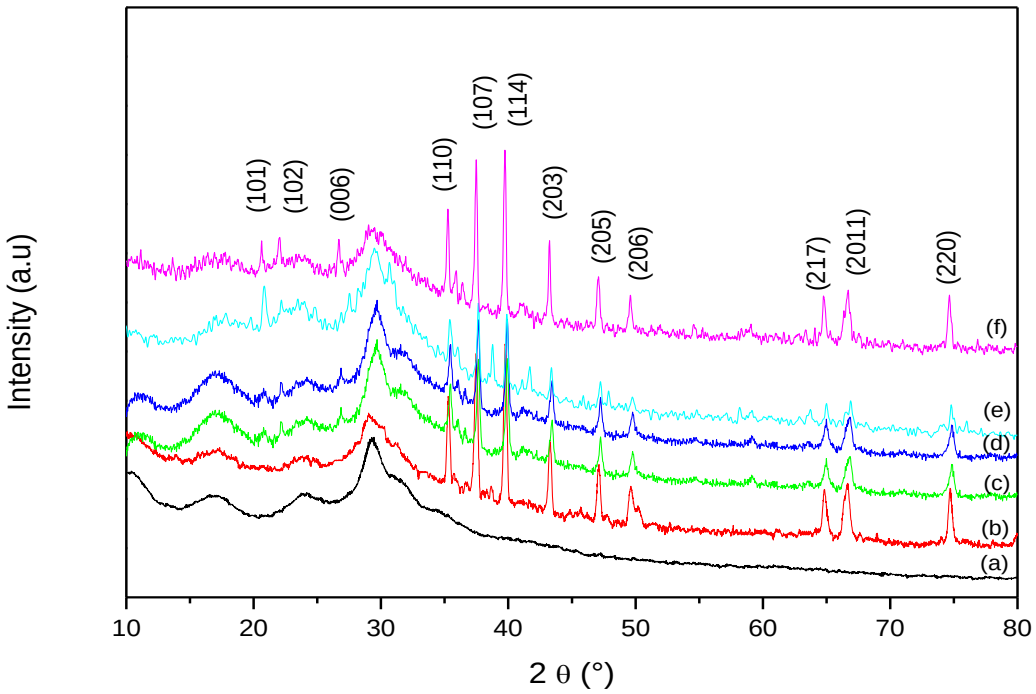
Intensity (a.u)
(101)
(102)
(006)
(110)
(107)
(114)
(203)
(205)
(206)
(217)
(2011)
(220)
(f)
(e)
(d)
(c)
(b)
(a)
10
20
30
40
50
60
70
80
2 θ (°)

Fig. 2.

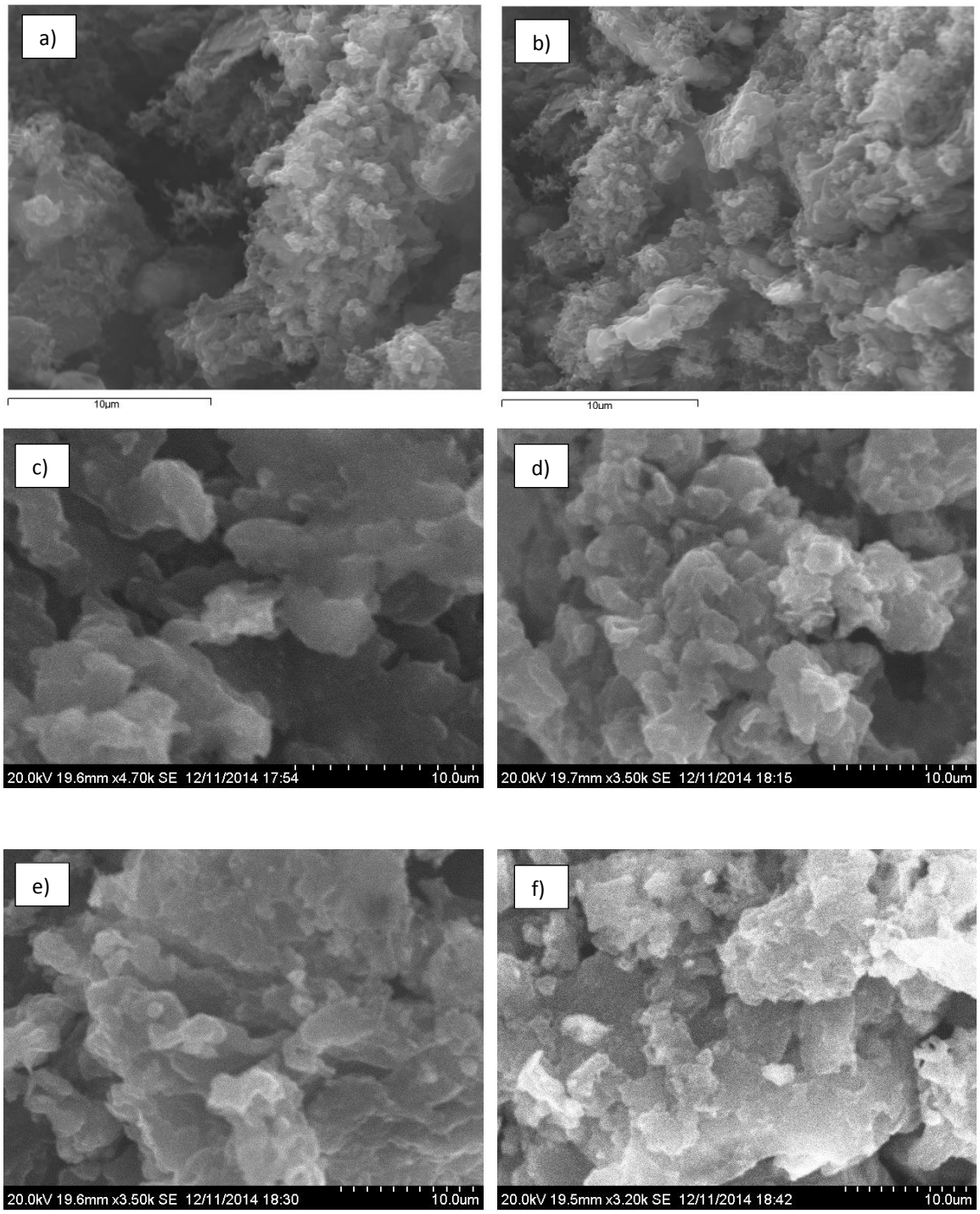
a)
10µm
b)
10um
c)
20.0kV 19.6mm x4.70k SE 12/11/2014 17:54
10.0um
d)
20.0kV 19.7mm x3.50k SE 12/11/2014 18:15
10.0um
e)
20.0kV 19.6mm x3.50k SE 12/11/2014 18:30
10.0um
f)
20.0kV 19.5mm x3.20k SE 12/11/2014 18:42
10.0um

Fig. 3.

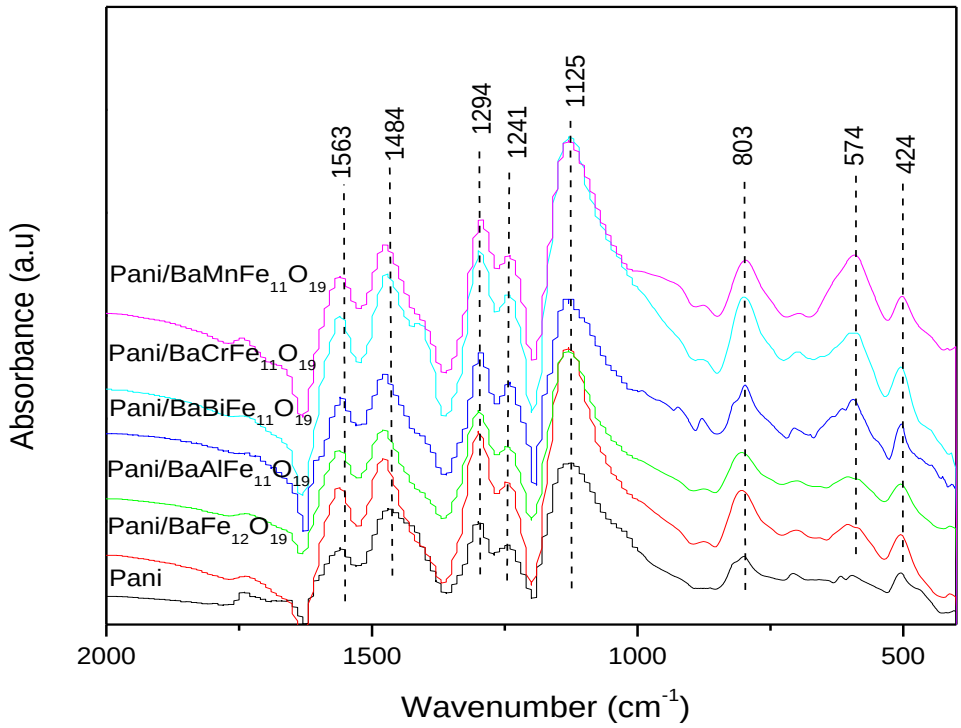
Absorbance (a.u)
1563
1484
1294
1241
1125
803
574
424
Pani/BaMnFe11O19
Pani/BaCrFe11O19
Pani/BaBiFe11O19
Pani/BaAlFe11O19
Pani/BaFe12O19
Pani
2000
1500
1000
500
Wavenumber (cm-1)

Fig. 4.

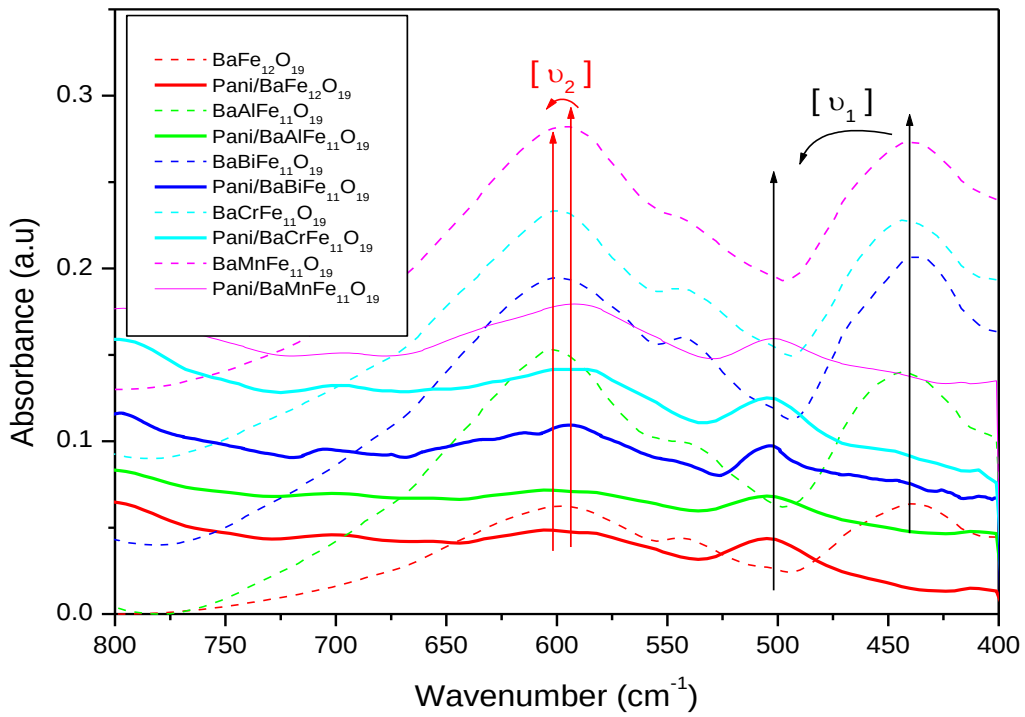
BaFe12O19
Pani/BaFe12O19
BaAlFe11O19
Pani/BaAlFe11O19
BaBiFe11O19
Pani/BaBiFe11O19
BaCrFe11O19
Pani/BaCrFe11O19
BaMnFe11O19
Pani/BaMnFe11O19
[υ2]
[υ1]
Absorbance (a.u)
0.0
0.1
0.2
0.3
800
750
700
650
600
550
500
450
400
Wavenumber (cm-1)

Fig. 5.

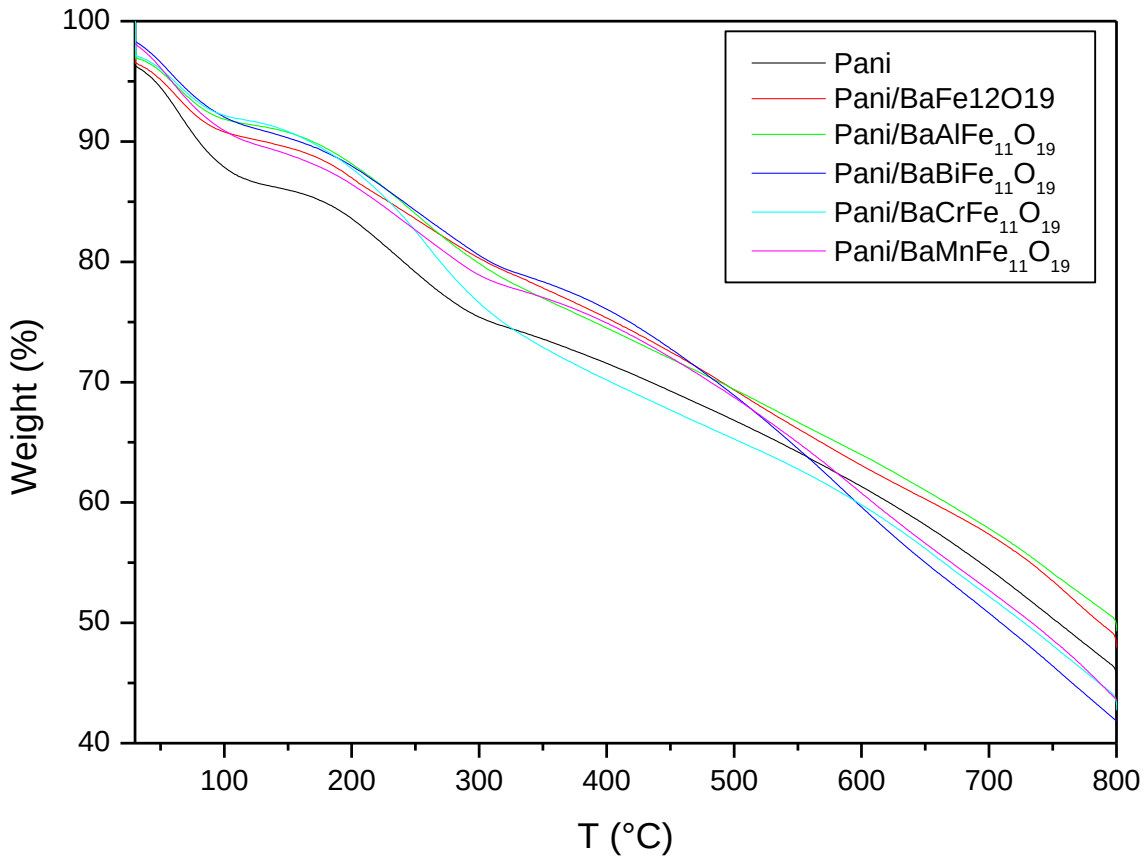
Pani
Pani/BaFe12O19
Pani/BaAlFe11O19
Pani/BaBiFe11O19
Pani/BaCrFe11O19
Pani/BaMnFe11O19
Weight (%)
T (°C)
100
90
80
70
60
50
40
100
200
300
400
500
600
700
800

Fig. 6.

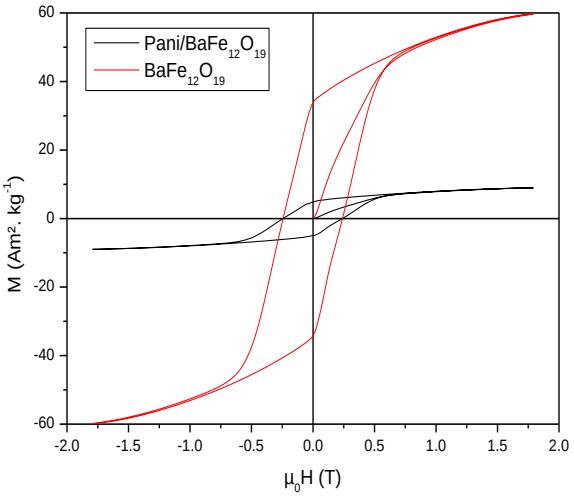
Pani/BaFe12O19
BaFe12O19
M (Am². kg-1)
μ0H (T)

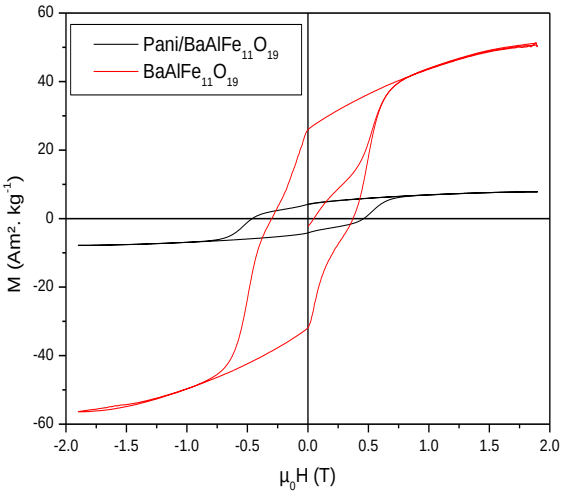
Pani/BaAlFe11O19
BaAlFe11O19
M (Am². kg-1)
μ0H (T)

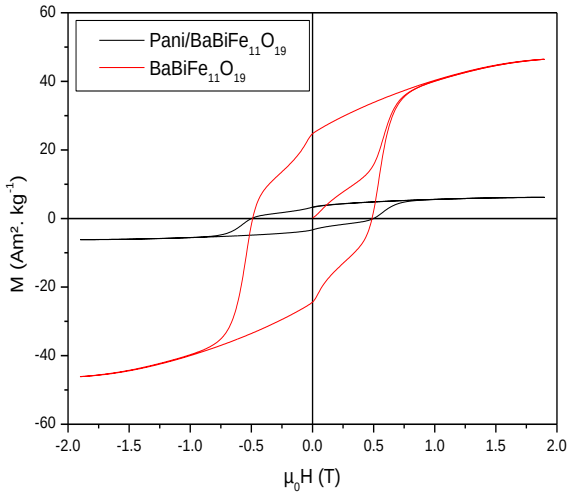
Pani/BaBiFe11O19
BaBiFe11O19
M (Am². kg-1)
μ0H (T)

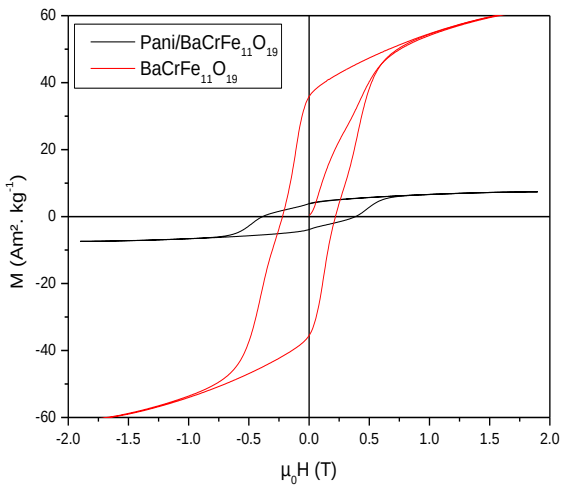
Pani/BaCrFe11O19
BaCrFe11O19
M (Am². kg-1)
μ0H (T)

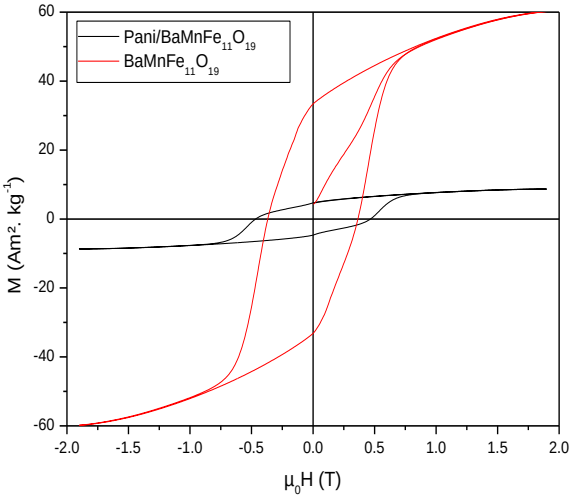
Pani/BaMnFe11O19
BaMnFe11O19
M (Am². kg-1)
μ0H (T)

Fig. 7.

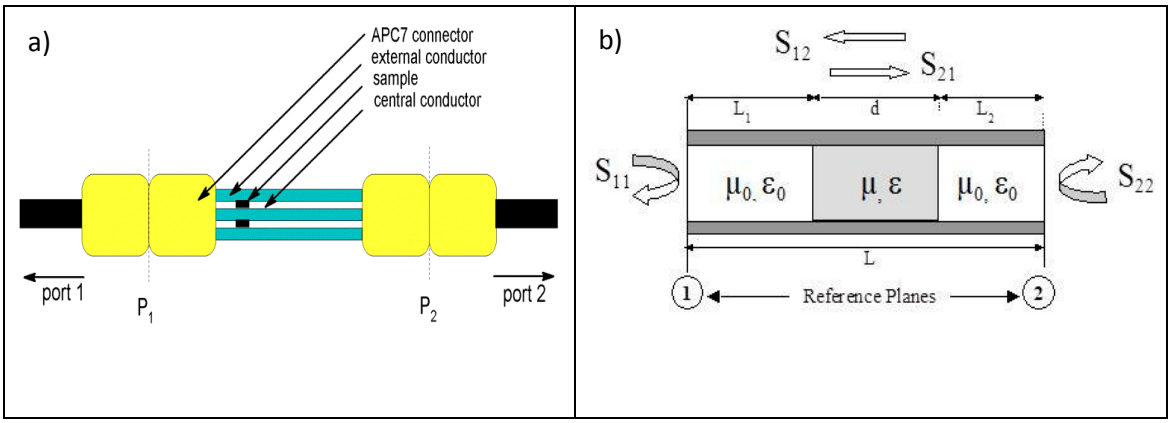
a)
APC7 connector
external conductor
sample
central conductor
port 1
P1
P2
port 2
b)
S12
S21
L1
d
L2
S11
μ0, ε0
μ, ε
μ0, ε0
S22
L
1
Reference Planes
2

Fig. 8.

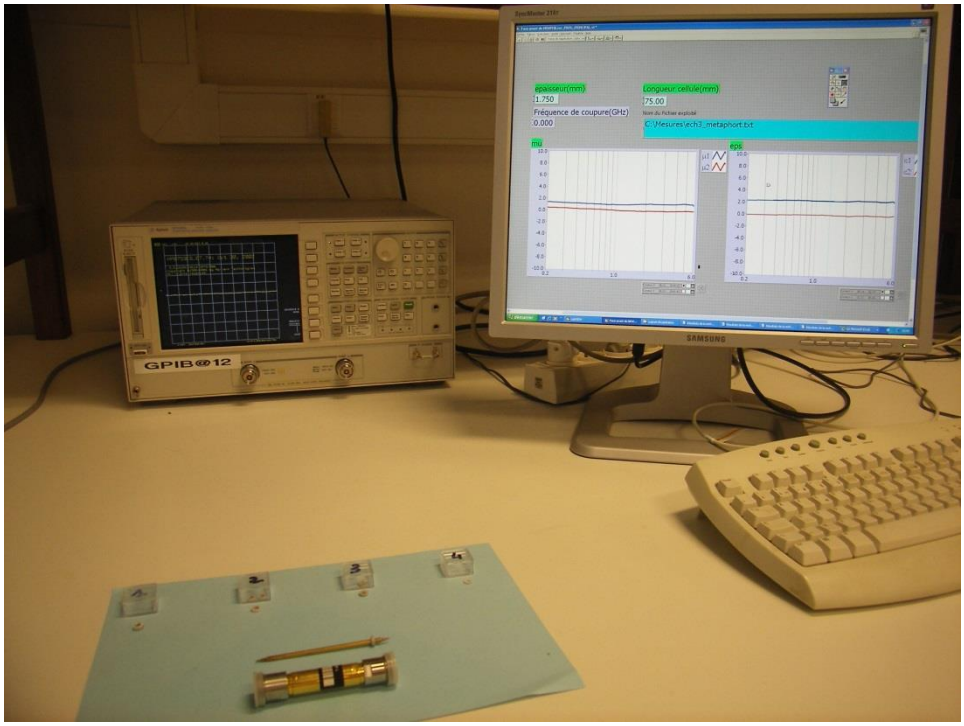
GPIB@12
epaisseur(mm)
1.750
Longueur cellule(mm)
75.00
Fréquence de coupure(GHz)
0.000
C:\Mesures\ech3_metaphort.txt
mu
eps
SAMSUNG

Fig. 9.

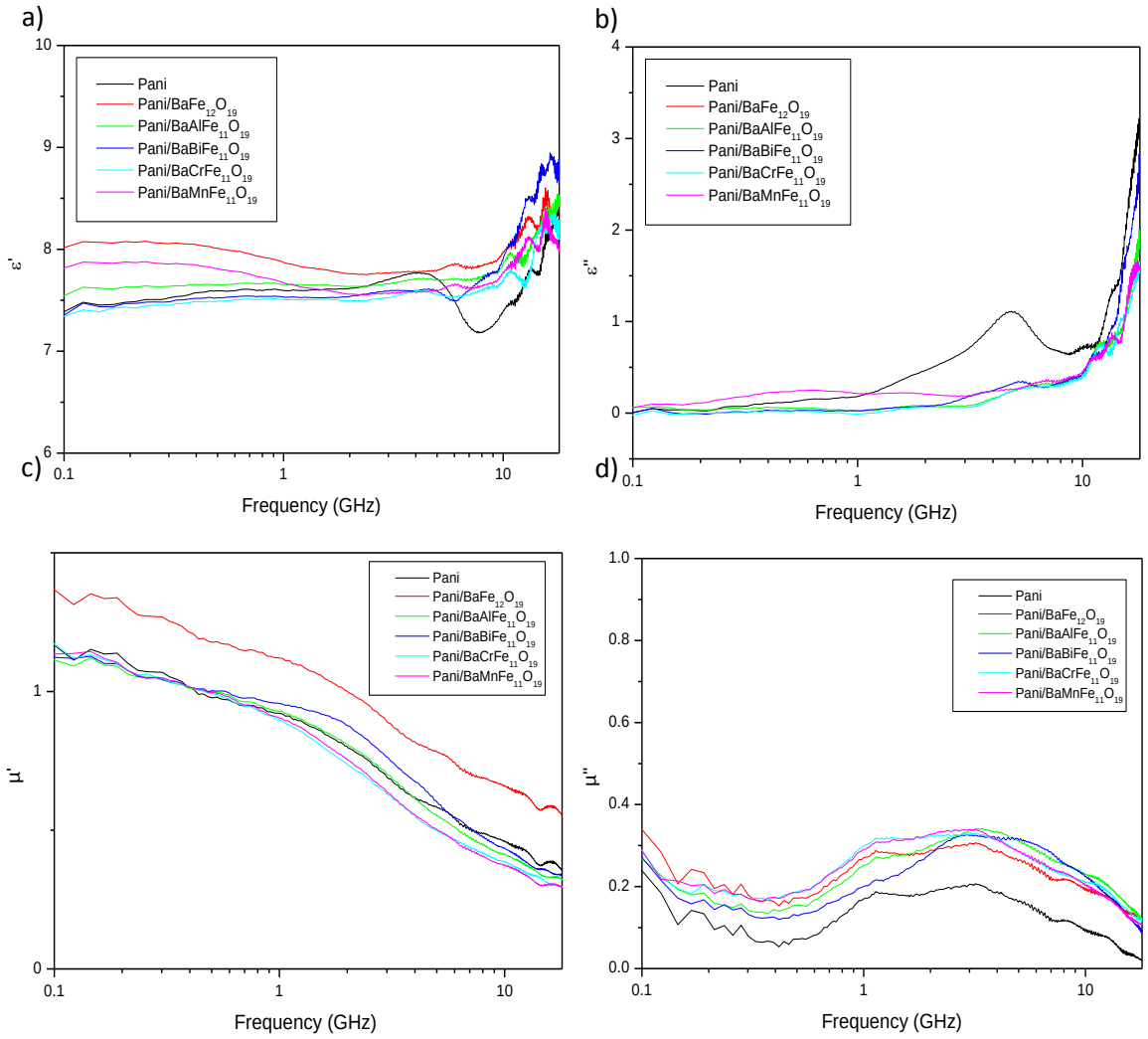
a)
b)
c)
d)
Pani
Pani/BaFe12O19
Pani/BaAlFe11O19
Pani/BaBiFe11O19
Pani/BaCrFe11O19
Pani/BaMnFe11O19
ε'
ε"
μ'
μ"
Frequency (GHz)

Fig. 10.

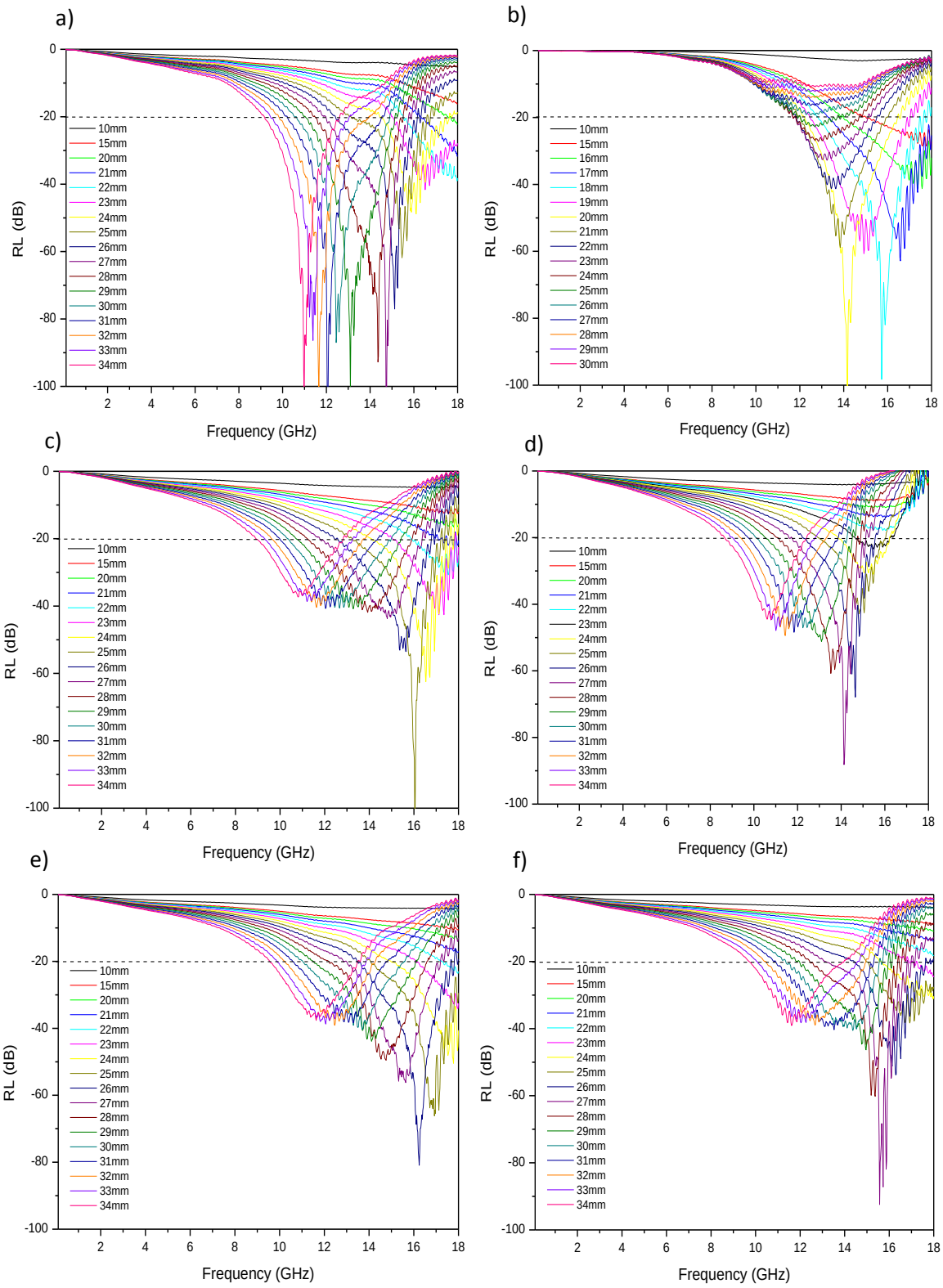
a)
b)
c)
d)
e)
f)
RL (dB)
Frequency (GHz)
10mm
15mm
16mm
17mm
18mm
19mm
20mm
21mm
22mm
23mm
24mm
25mm
26mm
27mm
28mm
29mm
30mm
31mm
32mm
33mm
34mm

Fig. 11.

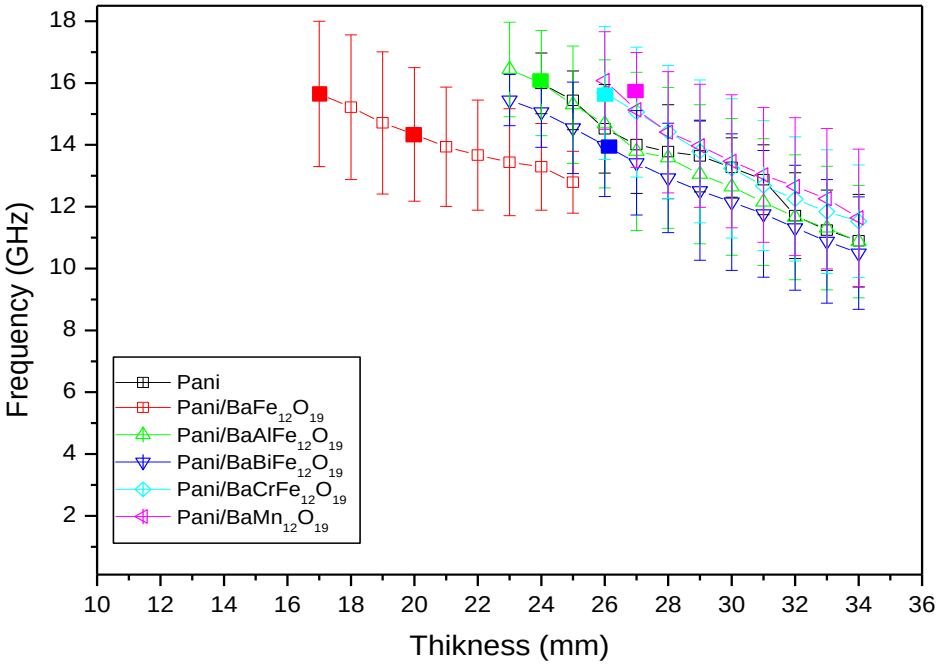
Frequency (GHz)
Thikness (mm)
Pani
Pani/BaFe12O19
Pani/BaAlFe12O19
Pani/BaBiFe12O19
Pani/BaCrFe12O19
Pani/BaMn12O19

Tables

Table 1

Sample	a (nm)	c (nm)	Crystallite size (nm)
Pani/$BaFe_{12}O_{19}$	0.58944	2.3231	294
Pani/$BaAlFe_{11}O_{19}$	0.58917	2.3181	183
Pani/$BaBiFe_{11}O_{19}$	0.58929	2.3185	229
Pani/$BaCrFe_{11}O_{19}$	0.58824	2.3212	252
Pani/$BaMnFe_{11}O_{19}$	0.58924	2.3193	215

Table 2

Vibrational assignments	Pani	Pani/ $BaFe_{12}O_{19}$	Pani/ $BaAlFe_{11}O_{19}$	Pani/ $BaBiFe_{11}O_{19}$	Pani/ $BaCrFe_{11}O_{19}$	Pani/ $BaMnFe_{11}O_{19}$
ν C=C (cm^{-1}) (quinoid rings)	1563	1567	1564	1562	1563	1565
ν C=C (cm^{-1}) (benzenoid rings)	1484	1488	1487	1485	1484	1485
ν C-N (cm^{-1})	1294	1297	1295	1296	1295	1297
ν N-H (cm^{-1})	1241	1243	1244	1241	1244	1247
ν N=Q=N mode (cm^{-1})	1125	1127	1129	1133	1132	1128
ν C-H out of plane (cm^{-1})	803	810	806	807	808	810
ν_2 (cm^{-1})	____	594	597	593	596	593
ν_1 (cm^{-1})	____	503	504	504	505	501

Table 3

Ion	Ionic radius (pm)	Molar mass (g. mol^{-1})
Fe^{3+}	67	55.8
Al^{3+}	57	27.3
Bi^{3+}	96	209.0
Cr^{3+}	64	52.0
Mn^{3+}	70	54.9

Table 4

Sample	1st weight loss (%)	2nd weight loss (%)	3nd weight loss (%)
Pani	9.2	11	31
Pani/$BaFe_{12}O_{19}$	5.5	10	37
Pani/$BaAlFe_{11}O_{19}$	5.3	13	40
Pani/$BaBiFe_{11}O_{19}$	6.2	11	38
Pani/$BaCrFe_{11}O_{19}$	5.2	15	35
Pani/$BaMnFe_{11}O_{19}$	7.1	12	36

Table 5

Sample	μ_0 Hc (T)	M_r ($Am^2.kg^{-1}$)	Ms at 1.8 T ($Am^2.kg^{-1}$)	Density ($g.cm^{-3}$)	w_{tHF}	w_{rHF}	Loading (%)
$BaFe_{12}O_{19}$	0.241	33.95	61.84	5.286	----	----	----
Pani/$BaFe_{12}O_{19}$	0.243	6.25	8.76	----	0.164	0.146	86
$BaAlFe_{11}O_{19}$	0.329	30.05	52.86	5.150	----	----	----
Pani/$BaAlFe_{11}O_{19}$	0.420	4.17	7.82	----	0.164	0.147	90
$BaBiFe_{11}O_{19}$	0.481	25.43	47.72	6.063	----	----	----
Pani/$BaBiFe_{11}O_{19}$	0.488	3.31	6.46	----	0.164	0.136	83
$BaCrFe_{11}O_{19}$	0.345	29.22	55.61	5.278	----	----	----
Pani/$BaCrFe_{11}O_{19}$	0.365	3.87	7.39	----	0.164	0.138	81
$BaMnFe_{11}O_{19}$	0.431	28.45	51.68	5.295	----	----	----
Pani/$BaMnFe_{11}O_{19}$	0.456	4.67	8.32	----	0.164	0.157	98